

Part II

Field Emission from Carbon Nanotubes

4 Field Emission Theory

Seungwu Han

4.1 Fowler–Nordheim Theory

Fowler and Nordheim (FN) first derived a semiclassical theory of field emission currents from cold metals in 1928 [1]. In this theory, the system is simplified as a one-dimensional structure along the direction of the external field. The emission tip is modeled as a semi-infinite quantum well with the work function of ϕ , and the local electric field (F) is approximated as a linear potential (Figure 4.1).

By employing the Wentzel–Kramers–Brillouin (WKB) approximation, the following FN equation was obtained:

$$J = 6.2 \times 10^{-6} \frac{\mu^{1/2}}{(\phi + \mu)^{1/2} \phi^{1/2}} F^2 \exp(-2.1 \times 10^8 \phi^{3/2}/F) \quad (4.1)$$

where J is in amperes per square centimeter of emitting surface, μ and ϕ are in volts, and F in volts per centimeter. Reordering the equation gives the FN plot as follows:

$$\log\left(\frac{J}{F^2}\right) = a - \frac{2.1 \times 10^8 \phi^{3/2}}{F} \quad \text{or} \quad \log\left(\frac{J}{V^2}\right) = a' - \frac{b'}{V} \quad (4.2)$$

where V is the applied bias voltage which is proportional to the local electric field F . The emission tip is geometrically sharp and the electric field is intensified at the tip end, producing a much higher local electric field than the macroscopic applied field. The ratio between the local and applied electric fields (F and E_a , respectively) is called the *field enhancement ratio* (β). For the nanotubes, β typically ranges between hundreds and thousands [2]. Since $\beta = F/E_a$, Eq. (4.2) can be rewritten as follows:

$$\log\left(\frac{J}{E_a^2}\right) = a'' - \frac{2.1 \times 10^8 \phi^{3/2}}{\beta E_a} \quad (4.3)$$

The above FN equation assumes a mathematically sharp surface–vacuum interface. In reality, the electron clouds from the metal do not terminate so sharply. In addition, the escaping electrons feel the image potential V_{im} exerted by the free electrons in the metal. In the classical expression, $V_{\text{im}} = -e^2/4x$, where x is

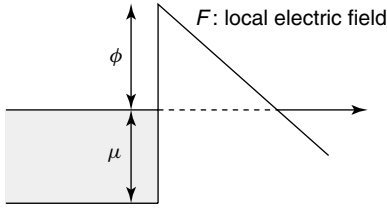


Figure 4.1 Schematic diagram to show the simplified model in the Fowler–Nordheim theory. The dashed line indicates the tunneling region.

the distance from the surface. (Note that, within a few angstroms from the tip, this formula should be modified to reflect the exchange-correlation effects.) The image potential effectively adds a multiplication factor in the exponent of Eq. (4.1) as a slowly varying function of F and can be regarded as a constant in most applications [3].

The FN theory has been successfully applied to numerous metallic systems even when the nonfree electrons such as d-band states are contributing to the carrier density. This is because the nonfree-electron-like states decay much faster than s-like free electrons because of the additional potential barrier associated with the spatial symmetry [4].

When the radii of the emitter tips are of the order of nanometers, the geometrical effects from the nonplanar shape should be taken into account. In [5], the image potentials depending on the tip geometry such as hyperboloid and cone were considered in calculating the one-dimensional tunneling currents within FN theory and the deviation from the linear FN behavior was noted (Figure 4.2). The resulting curve was well fitted to a formula including $1/V^2$ in the exponent as follows:

$$J = AV^2 \exp\left(-\frac{B}{V} - \frac{C}{V^2}\right) \quad (4.4)$$

4.2

Field Emission from CNTs

From the beginning of its discovery, the carbon nanotube has been regarded as an ideal material to make field emitters because of its unusually high aspect ratio as well as the mechanical and chemical stability. The semiclassical FN theory presented in the previous section has been very successful in many systems, not only for the planar geometry but also for small tips with the size of micrometers. As long as the radius of curvature is much higher than the wavelength of the electrons, the one-dimensional picture is a good approximation. However, in the nanostructures where the size of the tip is at most several times of the electron wavelength, such a simple scheme is not validated easily for the following reasons: First, the boundary of the tip is not a well-defined physical quantity in nanosize systems and the potential lines obtained through solving the Poisson equation will not be

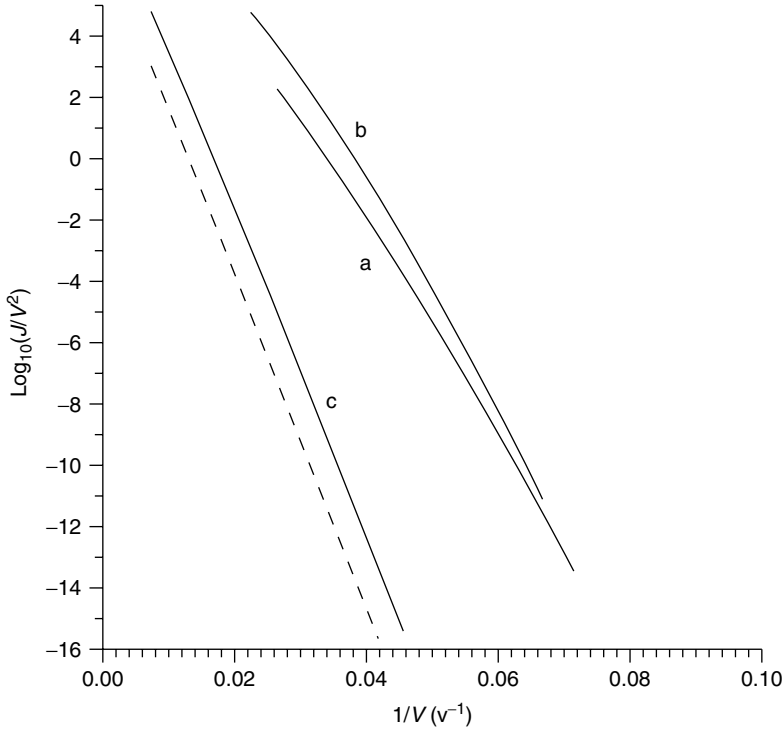


Figure 4.2 Fowler–Nordheim plots for the (a) hyperboloidal, (b) conical, and (c) planar tips. Nonlinearity is noticed for nonplanar geometries. The dashed line is the result from the FN formula. (Adapted from [5].)

valid at the atomic scale. In considering the emission process, the one-dimensional WKB approximation neglects the xy variations of the wave function as well as the potential. For example, the additional barriers felt by d-orbitals have been addressed in many experiments and theories [4]. The situation becomes more complicated in the nanotip where the dimension in the xy -plane is on the nanometer scale. It is also well known that the localized state induced by the adsorbates at the tip changes the currents dramatically [4]. In the nanotip, such localized states become relatively important as the number of channels for the metallic states is reduced because of the atomistic scale of the cross-sectional area. For carbon nanotubes, the localized states exist at the emission tip because of the topological constraint, and it was suggested that the defects can play an important role during the field emission [6]. The consideration of the localized states is rather clumsy in the semiclassical approach because they are not the current-carrying state.

Therefore, to quantitatively describe the field emission currents from the carbon nanotubes, a quantum mechanical approach considering the realistic three-dimensional atomic structure is required. So far, several methods have been

proposed to calculate the emission currents of the nanotubes. Below, we introduce them one by one with representative results.

4.2.1

Computational Methods to Calculate the Emission Currents from Carbon Nanotubes

4.2.1.1 The Integration of Time-Dependent Schrödinger Equation

In this method [7], the tunneling process is directly simulated by monitoring the time evolution of the wave functions. First, the first-principles calculations are performed on the nanotip under the electric field and the self-consistent potential and the wave functions are obtained. To confine the electronic charge within the emission tip during the self-consistency cycle, either a large barrier is applied temporarily outside the tip or, a localized basis set can be employed with the vacuum region is free of any basis. With the computed eigenstates as initial electronic configurations, the temporal wave functions are determined by solving the time-dependent Schrödinger equation. During the time evolution, the change of the electronic density is ignored to a first approximation and, therefore, the exchange and correlation potential is fixed with respect to the time. The transition rate of each state in the model nanotube tip is then evaluated from the amount of charge flowing out of the tip per unit time. The total current is obtained by summing up the product of the transition rate and the occupation number of individual states (Figure 4.3).

One advantage of this approach is that it can consider the tunneling process of both extended and localized states. (However, the extended states could be affected by the finite size effect of the model system.) It is noted that the localized states

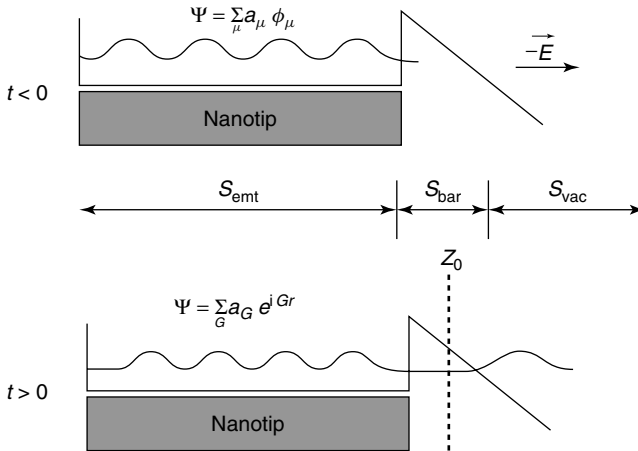


Figure 4.3 Schematic diagram to show the simulation of the tunneling process from nanotubes. Before $t < 0$, the wave functions are forced to be strictly inside the nanotube and the self-consistent potential

under the external field is obtained. At $t > 0$, the tunneling process of the electrons is described by integrating the time-dependent Schrödinger equation. (Adapted from [7].)

in the carbon nanotubes are orthogonal to the extended states and, therefore, the usual scattering formalism cannot capture the true tunneling rate for the localized states. It would be ideal if the contributions by the traveling states are evaluated within the Landauer–Büttiker formalism, while the tunneling of the localized states is described from the resonance width or the lifetime. One such approach was proposed in [8], but its application to nanotubes is yet to be performed.

When applied to the field emission of capped (5,5) and (10,10) carbon nanotubes, it was found that the emission currents from the localized states dominate the total current [7, 9]. The simulated image on the screen was dictated by the spatial symmetry of the localized states and displayed a pattern similar to that from the experiment [10] (Figure 4.4).

This approach has been applied to attack a wide range of problems in carbon nanotubes such as oxygen effects [11], BN-nanotube capping [12], double-wall carbon nanotubes [13], doping effects [14], metal nanowires [15], and field emission from alkali-doped BN nanotube [16]. The method was also applied to study the field emission from graphene nanoribbons [17].

4.2.1.2 Transfer Matrix Method

In this method [18], the Schrödinger equation is solved using the transfer matrix method. As shown in Figure 4.5, the whole system is divided into three regions: Region I ($z < -aN$) corresponds to a perfect metal. The intermediate region $-aN < z < 0$ contains N periodic repetitions of the unit cell that is not affected by the external fields. By forcing the incident waves travel through this finite length of the nanotube, the band structure effects can also be taken into the consideration. Region II ($0 < z < D$) contains the part of the nanotube subject to the electric field. The potential energy in region II is calculated by employing a pseudopotential for the ion-core potential in which the electronic density associated with the four

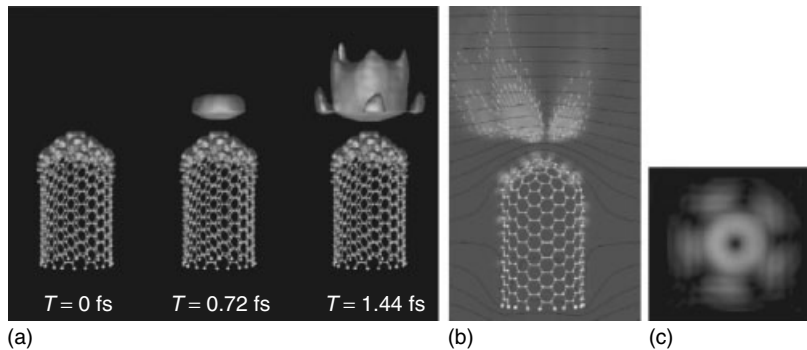


Figure 4.4 (a) Snapshots of the charge distribution of emitted electrons (doubly degenerate localized states) from the capped (10,10) nanotube. The amplitude of the wave function is magnified 30 times in the vacuum region for visual purpose. (b)

The current density of one of the localized states at the last instance of (a). The electronic density and the equipotential lines are also displayed. (c) The simulated image on the screen. (Adapted from [9].)

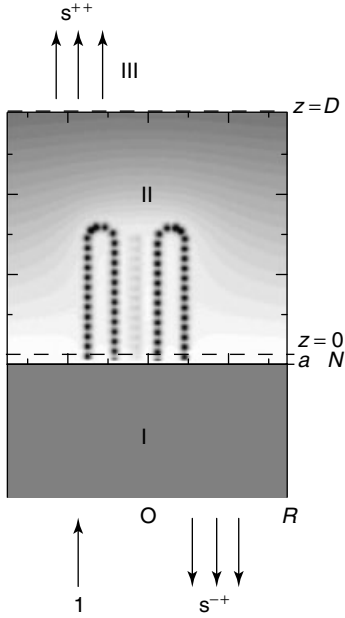


Figure 4.5 Schematic diagram depicting the transfer matrix method to calculate the field emission process. (Adapted from [18].)

valence electrons of each carbon atom is represented by the sum of Gaussian distributions. These electronic densities are displaced from the nuclear positions to reflect the screening of the external field and to produce dipole arrays. The region III ($z > D$) is the field-free vacuum.

By exploiting the cylindrical symmetry of the problem, the traveling states in region I and III can be expressed as follows:

$$\begin{aligned}\psi_{m,j}^{I,\pm} &= A_{m,j} J_m(k_{m,j}\rho) \exp(im\phi) \exp\left[\pm i\sqrt{(2m/\hbar^2) E - V_{\text{met}}z}\right] \\ \psi_{m,j}^{III,\pm} &= A_{m,j} J_m(k_{m,j}\rho) \exp(im\phi) \exp\left[\pm i\sqrt{(2m/\hbar^2) Ez}\right]\end{aligned}\quad (4.5)$$

where $A_{m,j}$ are normalization coefficients, J_m are Bessel functions, $k_{m,j}$ are wave vectors satisfying $J_m(k_{m,j}R) = 0$, E is the electron energy, and V_{met} is the potential energy in the metal in region I. Using Eq. (4.5), the scattering solutions in region I and III are given as follows:

$$\psi_{m,j}^+ = \begin{cases} \psi_{m,j}^{I,+} + \sum_{m',j'} S_{(m',j'),(m,j)}^{-+} \psi_{m',j'}^{I,-} & (z \leq -aN) \\ \sum_{m',j'} S_{(m',j'),(m,j)}^{++} \psi_{m',j'}^{III,-} & (z \geq D) \end{cases}\quad (4.6)$$

The connection between the coefficients is made through the transfer matrix formalism by dividing the system into thin slabs [19]. It is noted that this procedure

is not self-consistent in the sense that the scattering solutions do not affect the potential.

Using this approach, Mayer *et al.* compared the field emission properties of open and closed nanotubes in isolated or bundled configurations and found that the open tubes outperform the closed ones in the emission currents [18]. In addition, they also proposed a formula incorporating the number of tubes and the extraction field and found a deviation from the FN behavior at high electric fields. In [20], the field emission properties of single-wall and multiwall carbon nanotubes were also compared.

A similar approach uses the Lippmann–Schwinger equation [21], which was successfully applied to the field emission from a single-atom electron source [22]. In this case, the reference system is the vacuum–metal junction and the nanotube corresponds to the perturbation. The computational results on the (10,0) nanotube showed an emission distribution that is highly peaked at certain energies, indicating that those currents originate from the localized states at the tip region.

4.2.1.3 Other Quantum Mechanical Methods

Although not applied to carbon nanotubes, there have been several attempts to go beyond the conventional FN framework. In [8], Ishida *et al.* proposed an embedding Green function method which can incorporate the field emission current from both extended and localized states. The emission current from the extended states was calculated by the Landauer–Büttiker formula, while that from the localized states was estimated through the lifetime of the resonant states. In [23], a conventional scattering approach based on density functional theory was formulated and applied to study the field emission from the metal represented by the jellium model. Interestingly, the deviation from the FN plot was observed at high fields even for the planar tip geometry. For a realistic system, the method was applied to the field emission from the edges of the graphite ribbon arrays [24]. On the other hand, Ramprasad *et al.* introduced an approach based on the Bardeen transfer Hamiltonian method [25]. In particular, they employed the interpolated local density approximation (LDA) potential to address the image charge potential. Within this formalism, the left-hand side and the right-hand side (or cathode and anode) are calculated separately. The tunneling rate is then calculated using the wave function tails in the tunneling region and the Fermi golden rule.

4.2.1.4 Semiclassical Approaches

In the semiclassical approaches, the electronic structure of the nanotube tip is calculated at the three-dimensional quantum mechanical level but the transmission probability into the vacuum state is evaluated by WKB-style approximations. For example, in [26], the following form was developed for calculating the emission currents:

$$j(F, T) = \frac{1}{C} \sum_q \int_{BZ} N[E_q(k)] D[E_q(k), F] dk \quad (4.7)$$

where $N[E_q(k)]$ is the supply function given as the product of group velocity and the Fermi distribution function. $E_q(k)$ is the dispersion of the nanotube given below (the curvature effect is neglected):

$$E_q(k) = \pm t \sqrt{1 + 4 \cos\left(\frac{\sqrt{3}}{2} k_x a\right) \cos\left(\frac{k_y a}{2}\right) + 4 \cos^2\left(\frac{k_y a}{2}\right)} \quad (4.8)$$

where t is the hopping parameter, and k and q are quantum numbers running over the Brillouin zone of the nanotube. $D(E, F)$ is the tunneling probability through the one-dimensional potential barrier of the form $U(x, F) = \phi - e\beta Fx - e^2/4x$ and was evaluated by WKB approximation.

This approach has revealed many interesting properties of field emission of the nanotube that depend on the chirality. For example, the chiral effects were examined in [26], and it was found that the emission currents depend more on the energy gap than on the chirality (Figure 4.6). The intrinsic energy spectrum of the emitted electron was investigated and various subpeak features were found with respect to the applied bias and the temperature [27]. The field emission properties of multiwall nanotubes were also discussed in [28]. Recently, considering the energy band structure of the nanotube into account, an analytic expression for the generalized FN formula was also derived for the carbon nanotubes [29].

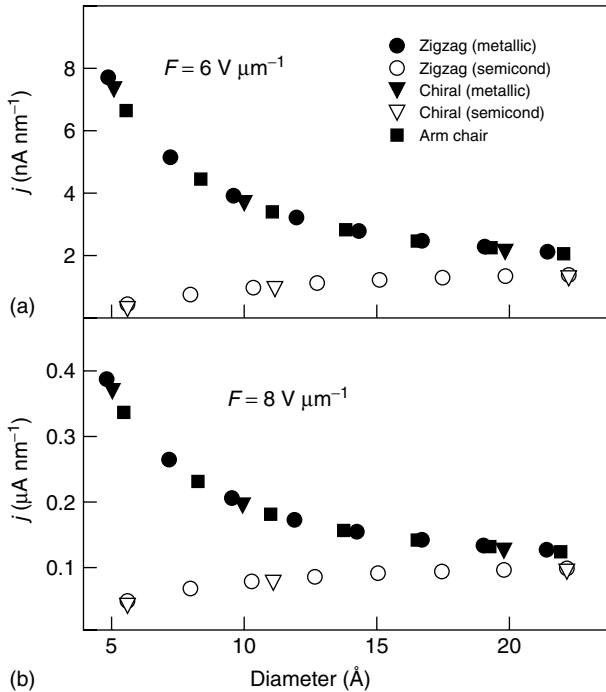


Figure 4.6 Current densities with respect to the diameter of the nanotube. (Adapted from [26].)

In the above method, the field emission process was approximated as one dimensional whereas the full band structure of the nanotube was considered within the tight-binding approximation. In the semiclassical method suggested in [30], the two-dimensional nature of the emitting surface was considered by dividing the supercell into a fine grid and calculating the emission currents along each grid point. This method is capable of evaluating the emission currents with spatial resolution on the plane normal to the emission direction, and therefore the projected image on the screen can be simulated (Figure 4.7).

4.2.2

Current–Voltage Characteristics of Field Emission Currents from Carbon Nanotubes

Several experiments have reported that the field emission currents from carbon nanotubes do not follow the straight FN plot and are rather saturated at high electric fields [31–34]. The nonlinear FN behavior was attributed to effects of space charge or molecules adsorbed at the emission tip. Theoretically, various results indicate that the nonlinear behavior could be intrinsic to the field emission from carbon nanotubes. In [35], the current saturation was attributed to the spatial distribution of electric fields that is specific to the nanotube. A similar result was obtained with more quantum mechanical treatment [36]. In [9], it was noted that the change of the occupation numbers corresponding to the highly emitting localized states slightly deflects the FN plot. On the basis of the explicit consideration of band structures in the nanotube, Liang *et al.* derived an analytical formula for the field emission from the carbon nanotubes (Figure 4.8) [29]. They attributed the non-FN behavior to the Dirac-electron behavior in the small-diameter, low-field region. Although not clarified quantitatively, the field penetration effect at the tip region may play a role in the nonlinear FN behavior, as has been demonstrated in the hybrid quantum mechanical approach on the realistic size of the nanotube [37].

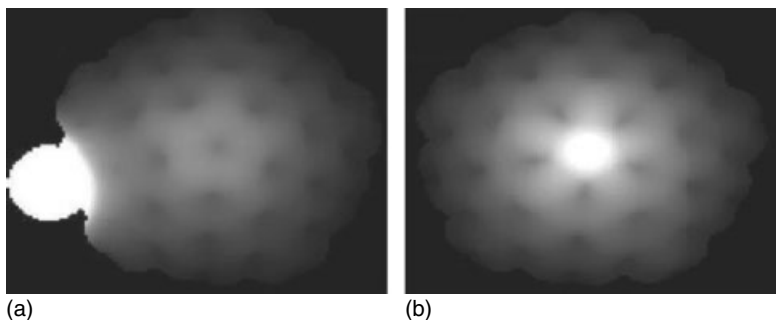


Figure 4.7 The tunneling probability patterns for the Cs adsorbed (a) and trapped (b) at the capped (10,10) nanotube. The external field is 0.3 V \AA^{-1} . (Adapted from [30].)

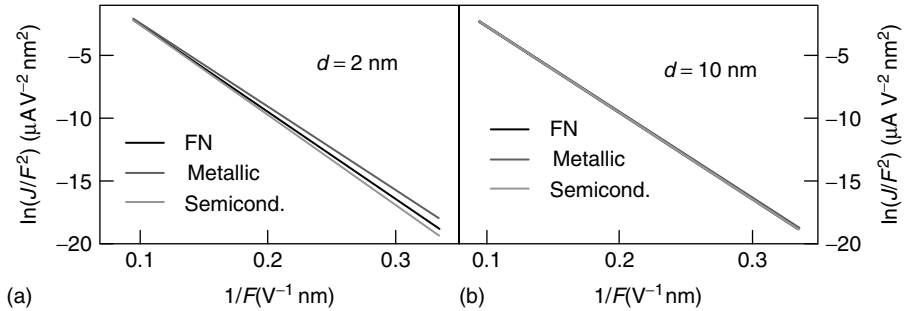


Figure 4.8 The FN plots of the emission currents from single-walled carbon nanotubes with various diameters. For the small-radius carbon nanotube, the deviation from the linear FN behavior is seen. (Adapted from [29].)

4.3 Concluding Remarks

Theoretically, the field emission from carbon nanotubes is a very challenging topic in many respects. Fundamentally, the field emission phenomena are highly nonequilibrium quantum mechanical processes that require the precise description of electronic structures of the nanotubes and the exponentially decaying tail of the tunneling electrons. As examined in this chapter, several approaches have been proposed so far, but none of them seems to provide the complete picture of the field emission of carbon nanotubes. For the refinement of the current methods and further development of new methodologies, feedback from experiments is critical. However, this has been hampered by the difficulties in isolating the emission current from a single carbon nanotube with well-defined geometry such as the length, radius, and chirality. Furthermore, the various possible configurations of pentagons that close the nanotube end will result in different current densities even among nanotubes with the same bulk structure. Therefore, advances in experiments to identify the emission currents from individual nanotubes will greatly assist the development of the theory.

References

1. Folwer, R.H. and Nordheim, L. (1928) Electron emission in intense electric fields. *Proc. R. Soc. London, Ser. A*, **119**, 173–181.
2. Edgcombe, C.J. and Valdrè, U. (2001) Microscopy and computational modeling to elucidate the enhancement factor for field electron emitters. *J. Microsc.*, **203**, 188–194.
3. Gomer, R. (1993) *Field Emission and Field Ionization, American Vacuum Society Classics*, American Institute of Physics, New York.
4. Gadzuk, J.W. and Plummer, E.W. (1973) Field emission energy distribution (FEED). *Rev. Mod. Phys.*, **45**, 487–548.
5. He, J., Cutler, P.H., and Miskovsky, N.M. (1991) Generalization of

- Fowler-Nordheim field emission theory for nonplanar metal emitters. *Appl. Phys. Lett.*, **59**, 1644–1646.
6. Han, S. and Ihm, J. (2000) Role of the localized states in field emission of carbon nanotubes. *Phys. Rev. B*, **61**, 9986–9989.
 7. Han, S., Lee, M.H., and Ihm, J. (2002) Dynamical simulation of field emission in nanostructures. *Phys. Rev. B*, **65**, 085405.
 8. Ishida, H., Wortmann, D., and Ohwaki, T. (2004) First-principles calculations of tunneling conductance. *Phys. Rev. B*, **70**, 085409.
 9. Han, S. and Ihm, J. (2002) First-principles study of field emission of carbon nanotubes. *Phys. Rev. B*, **66**, 241402.
 10. Saito, Y., Hata, K., and Murata, T. (2000) Field emission patterns originating from pentagons at the tip of a carbon nanotube. *Jpn. J. Appl. Phys.*, **39**, L271–L272.
 11. Park, N., Han, S., and Ihm, J. (2001) Effects of oxygen adsorption on carbon nanotube field emitters. *Phys. Rev. B*, **64**, 125401.
 12. Park, N., Han, S., and Ihm, J. (2003) Field emission properties of carbon nanotubes coated with boron nitride. *J. Nanosci. Nanotechnol.*, **3**, 179–183.
 13. Son, Y.-W., Oh, S., Ihm, J., and Han, S. (2005) Field emission properties of double-wall carbon nanotubes. *Nanotechnology*, **16**, 125–128.
 14. Ahn, H.-S., Lee, K.-R., Kim, D.-Y., and Han, S. (2006) Field emission of doped carbon nanotubes. *Appl. Phys. Lett.*, **88**, 093122.
 15. Lee, C.-K., Lee, B., Ihm, J., and Han, S. (2007) Field emission of metal nanowires studied by first-principles methods. *Nanotechnology*, **18**, 475706.
 16. Yan, B., Park, C., Ihm, J., Zhou, G., Duan, W., and Park, N. (2008) Electron emission originated from free-electron-like states of alkali-doped Boron-nitride nanotubes. *J. Am. Chem. Soc.*, **130**, 17012–17015.
 17. Tada, K. and Watanabe, K. (2002) Ab initio study of field emission from graphitic ribbons. *Phys. Rev. Lett.*, **88**, 127601.
 18. Mayer, A., Miskovsky, N.M., Cutler, P.H., and Lambin, Ph. (2003) Transfer-matrix simulations of field emission from bundles of open and closed (5,5) carbon nanotubes. *Phys. Rev. B*, **68**, 235401.
 19. Mayer, A. and Vigneron, J.-P. (1998) Quantum-mechanical theory of field electron emission under axially symmetric forces. *J. Phys.: Condens. Matter*, **10**, 869–881.
 20. Mayer, A., Miskovsky, N.M., and Cutler, P.H. (2002) Theoretical comparison between field emission from single-wall and multi-wall carbon nanotubes. *Phys. Rev. B*, **65**, 155420.
 21. Adessi, Ch. and Devel, M. (2000) Theoretical study of field emission by single-wall carbon nanotubes. *Phys. Rev. B*, **62**, 13314.
 22. Lang, N.D., Yacoby, A., and Imry, Y. (1989) Theory of a single-atom point source for electrons. *Phys. Rev. Lett.*, **63**, 1499–1502.
 23. Gohda, Y., Nakamura, Y., Watanabe, K., and Watanabe, S. (2000) Self-consistent density functional calculation of field emission currents from metals. *Phys. Rev. Lett.*, **85**, 1750–1753.
 24. Huang, S.F., Leung, T.C., Li, B., and Chan, C.T. (2005) First-principles study of field-emission properties of nanoscale graphite ribbon arrays. *Phys. Rev. B*, **72**, 035449.
 25. Ramprasad, R., Fonseca, L.R.C., and Allmen, P. (2000) Calculation of the field-emission current from a surface using the Bardeen transfer Hamiltonian method. *Phys. Rev. B*, **62**, 5216–5220.
 26. Liang, S.-D., Huang, N.Y., Deng, S.Z., and Xu, N.S. (2004) Chiral and quantum size effects of single-wall carbon nanotubes on field emission. *Appl. Phys. Lett.*, **85**, 813–815.
 27. Liang, S.-D., Huang, N.Y., Deng, S.Z., and Xu, N.S. (2006) Intrinsic energy spectrum in field emission of carbon nanotubes. *Phys. Rev. B*, **73**, 245301.
 28. Liang, S.-D., Deng, S.Z., and Xu, N.S. (2006) Seeking optimal performance of multiwall carbon nanotubes in field emission: tight-binding approach. *Phys. Rev. B*, **74**, 155413.

29. Liang, S.-D. and Chen, L. (2008) Generalized Fowler-Nordheim theory of field emission of carbon nanotubes. *Phys. Rev. Lett.*, **101**, 027602.
30. Khazaei, M., Farajian, A.A., and Kawazoe, Y. (2005) Field emission patterns from first-principles electronic structures: application to pristine and cesium-doped carbon nanotubes. *Phys. Rev. Lett.*, **95**, 177602.
31. Bonard, J.-M., Salvetat, J.-P., Stöckli, T., Forró, L., and Châtelain, A. (1999) Field emission from carbon nanotubes: perspectives for applications and clues to the emission mechanism. *Appl. Phys. A*, **69**, 245–254.
32. Collins, P.G. and Zettl, A. (1996) A simple and robust electron beam source from carbon nanotubes. *Appl. Phys. Lett.*, **69**, 1969–1971.
33. Collins, P.G., and Zettl, A. (1997) Unique characteristics of cold cathode carbon-nanotube-matrix field emitters. *Phys. Rev. B*, **55**, 9391–9399.
34. Xu, X. and Brandes, G.R. (1999) A method for fabricating large-area, patterned, carbon nanotube field emitters. *Appl. Phys. Lett.*, **74**, 2549–2551.
35. Buldum, A. and Lu, J.P. (2003) Electron field emission properties of closed carbon nanotubes. *Phys. Rev. Lett.*, **91**, 236801.
36. Peng, J., Li, Z., He, C., Chen, G., Wang, W., Deng, S., Xu, N., Zheng, X., Chen, G., Edgcombe, C.J., and Forbes, R.G. (2008) The roles of apex dipoles and field penetration in the physics of charged, field emitting, single-walled carbon nanotubes. *J. Appl. Phys.*, **104**, 014310.
37. Zheng, X., Chen, G., Li, Z., Deng, S., and Xu, N. (2004) Quantum-mechanical investigation of field-emission mechanism of a micrometer-long single-walled carbon nanotube. *Phys. Rev. Lett.*, **92**, 106803.